HW3 - Network Dynamics

Luciano Scarpino - s346205

January 2026

Collaborators (on all tasks):

S346378	Salvatore Nocita
S334015	Andrea Vasco Grieco
S329057	Shadi Mahboubpardahi

We discussed the project and worked jointly on each exercise.

Exercise 1

Reminder about SIR epidemics

SIR epidemics are models in which each node can take one of three states:

1. Susceptible: when in this state a node can be infected
2. Infected: when in this state a node can spread the epidemics to other susceptible nodes, making them infected as well
3. Recovered: when in this state a node can neither get infected nor infect other nodes

In our simulations we assume that the probability that an infected node spreads the disease to an adjacent node is $\beta \in [0, 1]$ while the probability that an infected node recovers is $\rho \in [0, 1]$. Moreover, we will assume that at any point in t in time, nodes are in state $X_i(t) \in \{\text{S, I, R}\}$, denoting respectively the *susceptible, infected* and *recovered*. Therefore, we can formally write that:

$$\mathbb{P}(X_i(t+1) = I \mid X_i(t) = S, \sum_{j \in \mathcal{V}} W_{ij}\, \delta^I_{X_j(t)} = m) = 1 - (1-\beta)^m,$$
$$\mathbb{P}(X_i(t+1) = R \mid X_i(t) = I) = \rho.$$

where $\sum_{j \in \mathcal{V}} W_{ij}\, \delta^I_{X_j(t)}$ denotes the number of infected neighbors for node i.

Problem 1.1: simulation on a k-regular graph

In this section we simulate an SIR epidemic on a k-regular graph. We start by creating a k-regular graph with $k = 4$ and a total number of nodes $n = 500$. This is an undirected graph in which each node $i \in \{1, \dots, n\}$ is connected to the two nodes that are immediately before and after itself and to nothing else, meaning that each node has exactly degree k. In our simulation we set $\beta = 0.3$ and $\rho = 0.7$, and perform the simulation for 15 timesteps, assuming that each one of them represents a week. At time $t = 0$ we assume that 10 nodes are infected, selecting them at random from the node set $\mathcal{V}$, and perform the simulation $N = 100$ times.

The results of the simulation are shown in Figure 1. In particular, Figure 1a shows that every week the number of new infected decreases.

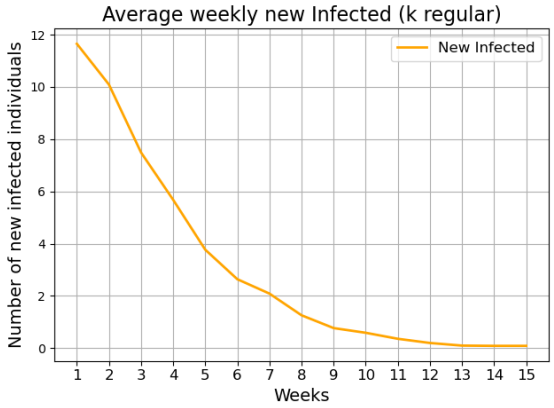

(a) Weekly new infected, averaged over $N = 100$ simulations

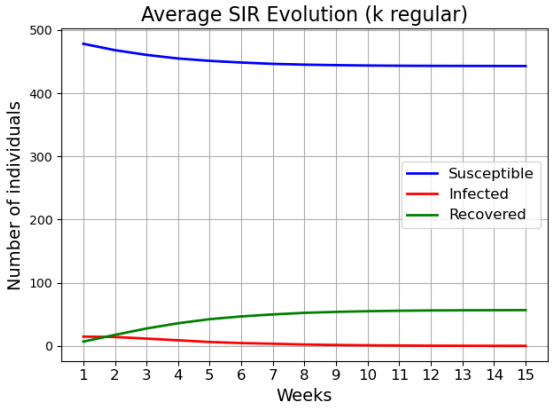

(b) Weekly evolution of susceptible, infected and recovered, averaged over $N = 100$ simulations

Figure 1: Results of the simulation of an epidemic on a k regular graph over 15 weeks, without vaccination and with $k = 4$ and population $n = 500$. Plots are averaged over $N = 100$ simulations

We can better understand the context of this evolution by looking at Figure 1b and observe that the final equilibrium is composed by less than 100 recovered nodes, while most of the population remains susceptible, and is therefore never reached by the infection. This is likely due to the interplay between the two stochastic parameters ρ and β on the structure of the graph. We first want to observe that the only source of randomness is given by these parameters, given that the graph is fixed (differently from what will happen in the next exercises). Furthermore, k-regular graphs have limited connectivity due to the absence of hubs, i.e. nodes with higher degree, that have a larger probability of spreading the infection. So the structure of the graph itself makes it resilient to the spread of epidemics.

This behavior is also increased by the relatively high probability of recovery after one week (70%) and the relatively small probability of infection, in the context of the low connectivity of the graph.

Problem 1.2: creating a preferential attachment graph

In this section we write a simple function to generate a preferential attachment graph with n nodes and average degree $k \in \mathbb{Z}^+$. The pseudocode is reported in Algorithm 1.

Problem 2: simulating a pandemic without vaccination

In this section we use the preferential attachment graph to simulate a pandemic without vaccination. In particular we use as parameters $k = 6$, $\beta = 0.3$, $|\mathcal{V}| = 500$ and $\rho = 0.7$ for 15 weeks. We start by sampling 10 infected nodes at random for the initial configuration. Figure 2 shows the results of the simulations. In particular, we can observe from Figure 2a an initial spike in the number of new infected individuals. While this is certainly facilitated by the higher average degree, compared to the one from problem 1, this fact alone would not be enough to explain this picture. Once again, one of the main factor has to do with the structure of the preferential attachment graph. In fact, it is constructed in such a way that it tends to create hubs. These are nodes with connectivity that is significantly higher than the average $k = 6$. For instance, in our case we obtained a graph whose largest degree was 73.

Such a radically different structure, helps explain this plot: whenever some of these hubs are infected they facilitate the spreading of the disease, causing the initial spike in the number of new infected.

Algorithm 1 Pseudocode to create a preferential attachment graph with average degree $k \in \mathbb{Z}^+$

Require: Total number of nodes N, desired average degree $k \in \mathbb{Z}^+$
Ensure: Graph $G = (V, E)$
  Initialize G as a complete graph on $k+1$ nodes
  $a \leftarrow 0$ ▷ Auxiliary variable for odd degree alternation
  for $i = k+1, \ldots, N-1$ **do**
    Compute degrees $d_j = \deg(j)$ for all $j \in V$
    Compute attachment probabilities $p_j = d_j / \sum_{v \in \mathcal{V}} d_v$

    if k is odd **then** ▷ Alternate between floor and ceil if k is odd
      $a \leftarrow 1 - a$
    else
      $a \leftarrow 0$
    end if
    $m \leftarrow \lfloor k/2 \rfloor + a$
    Sample m distinct nodes $T \subset \mathcal{V}$ according to probabilities $\{p_j\}$
    for each $j \in T$ **do**
      Add edge (i, j) to G
    end for
  end for
  return G

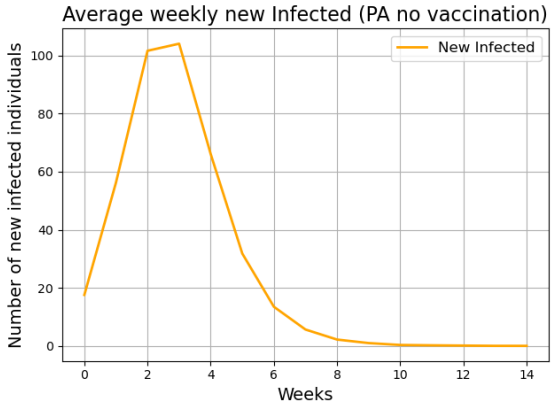

(a) Weekly new infected, averaged over $N = 100$ simulations

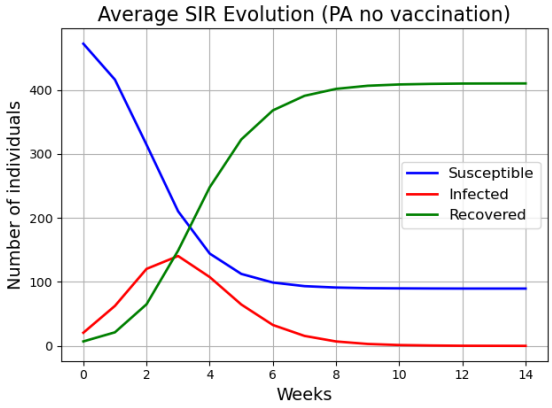

(b) Weekly evolution of susceptible, infected and recovered, averaged over $N = 100$ simulations

Figure 2: Results of the simulation of an epidemic on a preferential attachment graph over 15 weeks, without vaccination with $k = 6$ and population $n = 500$. Plots are averaged over $N = 100$ simulations

To better understand the sharp decrease, we can refer to Figure 2b. We can see that the number of recovered increases rapidly, and it is only slightly delayed compared to the infected people. In particular, the epidemic ends while leaving about 20% of the population in a susceptible state, mostly due to the shielding effect that the recovered exert, protecting the remaining susceptible population. It should be noted that most of the population (80%) becomes infected at some point during the weeks, as shown by the curve of the recovered.

Problem 3: simulating a pandemic with vaccination

We perform the same simulation as before introducing vaccination. In particular, we assume that the percentage of the total population that received vaccination is described by the following vector:

$$\text{Vacc(t)} = [0, 5, 15, 25, 35, 45, 55, 60, 60, 60, 60, 60, 60, 60, 60]$$

under the assumption that vaccines are immediately effective and that they are given uniformly in the population, even to recovered and infected people. In the former case it has no effect, in the latter it makes the node incapable of infecting. Intuitively, we would expect the vaccination campaign to mitigate the number of people that get infected.

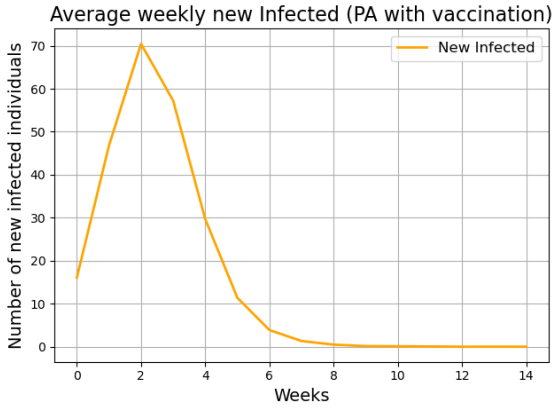

(a) Weekly new infected, averaged over $N = 100$ simulations

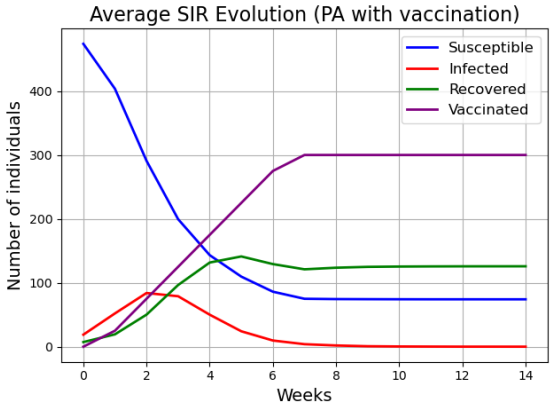

(b) Weekly evolution of susceptible, infected and recovered, averaged over $N = 100$ simulations

Figure 3: Results of the simulation of an epidemic on a preferential attachment graph over 15 weeks with vaccination and with $k = 6$ and population $n = 500$. Plots are averaged over $N = 100$ simulations

The average results of the simulations are depicted in Figure 3. Let us start by comparing Figure 3a with Figure 2a. We can observe that, while the shape presents a similar initial increase followed by a stark decrease, when vaccines are present the peak is significantly lower. In fact, without vaccinations the newly infected curve peaked at more than 100, while in this case it peaked at around 70 new weekly infected. Moreover, the decrease after week 2 in the curve of the new contagions is steeper in the case with vaccinations, consistently with our expectations.

We can now analyze Figure 3b. Observe that the curve of the total infected people is more blunt compared to the one observed in Problem 3. The numbers of both recovered and susceptible are lower, because they have been partially absorbed by the vaccinated people. This is indeed a limit of our simulation, because this plot is no longer enough to understand how many people actually got in contact with the infection, as the recovered people no longer match that information precisely. However, simply summing the values of Figure 3a and adding the initial 10 infected nodes tells us that, on average, 247.66 people got infected at some point. Adopting the same procedure in Problem 2 yield the value of 410.39. Indeed, this means that only about 50% of the population got exposed to the virus, compared to the 80% of the case without vaccination.

Problem 4: The H1N1 pandemic in Sweden

We will now try to simulate the H1N1 pandemic in Sweden between week 42, 2009 and week 5, 2010. We will reduce the total population to $n = |\mathcal{V}| = 934$, scaling the Sweden population down by a factor

of 10^4. During this period we will use this data:

$$\text{Vacc(t)} = [5, 9, 16, 24, 32, 40, 47, 54, 59, 60, 60, 60, 60, 60, 60]$$
$$I_0(t) = [1, 1, 3, 5, 9, 17, 32, 32, 17, 5, 2, 1, 0, 0, 0, 0]$$

where once again the i-th entry of Vacc(t) denotes the percentage of the population that was vaccinated by week i and each entry of $I_0(t)$ denotes the number of people that got infected in the corresponding week, hence it contains the number of new weekly infected people. Notice that the first entry of $I_0(t)$ contains the initial value of infected. Furthermore, we assume the data of Vacc(t) to go from week 43,2009 to week 5, 2010, while we assume that the data in $I_0(t)$ goes from week 42, 2009 to week 5, 2010 and the first number is the starting value of infected people.

We assume that we can model the epidemic with a preferential attachment graph. However, this is different from the previous situation given that optimal values for β, ρ and k are not known in advance. To estimate them, we can use the method shown in Algorithm 2.

In particular, we initialize the parameters $k_0 = 10, \beta_0 = 0.3, \rho_0 = 0.6$ and $\Delta k = 1$, $\Delta\beta = 0.1$ and $\Delta\rho = 0.1$. To estimate the quality of the performance we create 30 different preferential attachment graphs and perform 1000 simulations on each, in order to get a reliable estimate of the RMSE.

In our simulation with Algorithm 2 we achieve convergence in just 3 iterations. The improvement over the initial guess is substantial: we managed to reduce the RMSE from 42.489 to 6.149.
The values at which the algorithm converged are $k = 8$, $\beta = 0.2$ and $\rho = 0.6$.

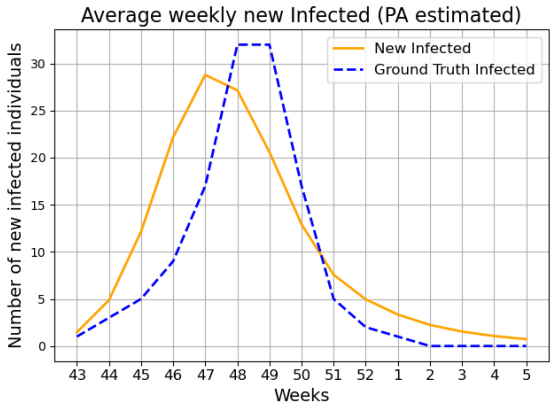

(a) Weekly new estimated infected compared with the ground truth $I_0(t)$, averaged over $N = 1000$ simulations and 30 graphs

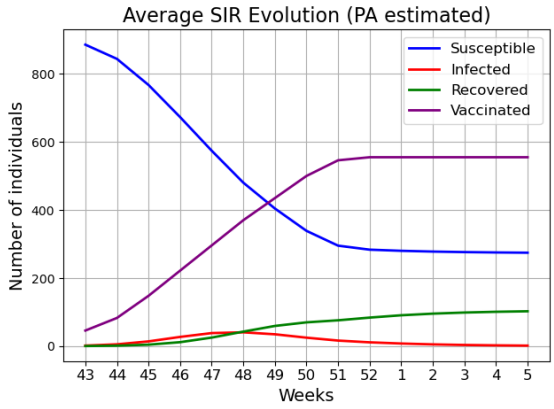

(b) Weekly evolution of susceptible, infected and recovered, averaged over $N = 100$ simulations and 30 graphs

Figure 4: Results of the simulation with preferential attachment with $k = 8$, $\beta = 0.2$ and $\rho = 0.6$ (as estimated by Algorithm 2). Results are averaged over $N = 100$ simulations and 30 graphs

In Figure 4 we can observe the plots of our simulation and a comparison with the ground truth data $I_0(t)$. Notice that both Figure 4a and Figure 4b start at week 43. In fact, we assume that the first week (i.e. week 42) only serves as a starting point for the infections, but there is no point in showing it, given that we lack other information, as, for instance, the number of vaccinated people. We can see that the estimated curve of the new infected in Figure 4a has a shape that is similar to the one of $I_0(t)$, but it seems to be starting and decreasing too early, meaning it looks translated to the left. Moreover, the steepness of the growth and decrease are slightly less than the ground truth.

In Figure 4b we can observe the simulation of the epidemic with the weekly average number of the population states. We can see that about a third of the population never encounters the infection and

Algorithm 2 Grid-based parameter search for network and epidemic model calibration

Require: Initial parameters (k_0, β_0, ρ_0), step sizes $(\Delta k, \Delta\beta, \Delta\rho)$, maximum number of iterations `max_iter`
Require: Number of simulations $N_{\text{sim}} = 10$, ground truth data $\{I_0(t)\}_{t=1}^{15}$
Ensure: Estimated parameters (k^*, β^*, ρ^*)

converged $\leftarrow$ **false**
while not converged **do**
  $\text{RMSE}_{\min} \leftarrow +\infty$
  $(k^*, \beta^*, \rho^*) \leftarrow (k_0, \beta_0, \rho_0)$
  `it_counter` $\leftarrow 0$
  for $k \in \{k_0 - \Delta k,\ k_0,\ k_0 + \Delta k\}$ **do**
    for $\beta \in \{\beta_0 - \Delta\beta,\ \beta_0,\ \beta_0 + \Delta\beta\}$ **do**
      for $\rho \in \{\rho_0 - \Delta\rho,\ \rho_0,\ \rho_0 + \Delta\rho\}$ **do**
        `it_counter` $\leftarrow$ `it_counter` $+ 1$
        Generate a preferential attachment graph $G = (\mathcal{V}, \mathcal{E})$
          with $|\mathcal{V}| = 934$ nodes and average degree k
        for $i = 1, \ldots, N_{\text{sim}}$ **do**
          Simulate the pandemic on G from week 42 for 15 weeks
            using parameters (β, ρ) and the vaccination scheme
          Record weekly new infections $I_i(t)$
        end for
        Compute average weekly infections: $I(t) \leftarrow \frac{1}{N_{\text{sim}}} \sum_{i=1}^{N_{\text{sim}}} I_i(t)$
        Compute RMSE: $\text{RMSE} \leftarrow \sqrt{\frac{1}{15} \sum_{t=1}^{15} \big(I(t) - I_0(t)\big)^2}$
        if $\text{RMSE} < \text{RMSE}_{\min}$ **then**
          $\text{RMSE}_{\min} \leftarrow \text{RMSE}$
          $(k^*, \beta^*, \rho^*) \leftarrow (k, \beta, \rho)$
        end if
      end for
    end for
  end for
  if $(k^*, \beta^*, \rho^*) = (k_0, \beta_0, \rho_0)$ or `it_counter` $\geq$ `max_iter` **then**
    converged $\leftarrow$ **true**
  else
    $(k_0, \beta_0, \rho_0) \leftarrow (k^*, \beta^*, \rho^*)$
  end if
end while
return (k^*, β^*, ρ^*)

is not vaccinated. Moreover, the total number of infected people peaks around week 47 with a value that looks well below 100 and then decreases.

Initial improvements on the algorithm: adaptively reducing the amplitude of the search space

We tried to improve the quality of the estimate by enlarging the initial values of Δk, $\Delta\beta$ and $\Delta\rho$ and every time we encountered a repetition of the parameters, as in line 26 of Algorithm 2, we halved them instead of stopping the estimation. It would also be possible to set a maximum number of halvings or a threshold for each interval, however for this testing we simply ran the optimization for 100 iterations. The only point to notice is that we restricted $\Delta k \in \mathbb{Z}^+$. The final values of the convergence are shown in Table 1.

	Algorithm 2	Algorithm 2 with adaptive halving
k^*	8	7
β^*	0.2	0.225
ρ^*	0.6	0.588
RMSE	6.149	**6.084**

Table 1: Results of the optimization using Algorithm 2 and the proposed adaptive method, performing halving of Δk, $\Delta\beta$ and $\Delta\rho$ whenever a repetition is encountered over 100 iterations.

Notice that the both the RMSE and the convergence values are similar, and therefore there is no evidence that this simple method improved the simulation at all.

However, we can obtain some interesting insights on the convergence process by inspecting Figure 5. In particular, we can observe from 5a that the RMSE does not really decrease past the first few

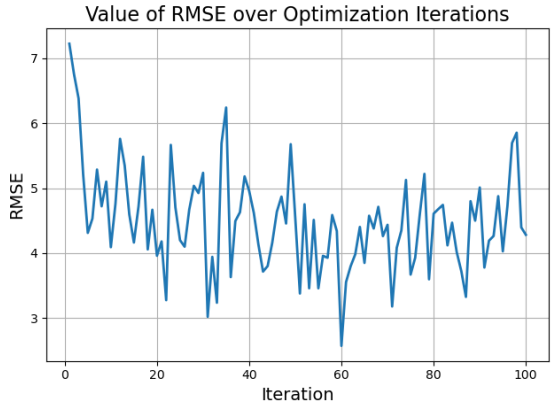

(a) RMSE error of the optimization algorithm through 100 iterations

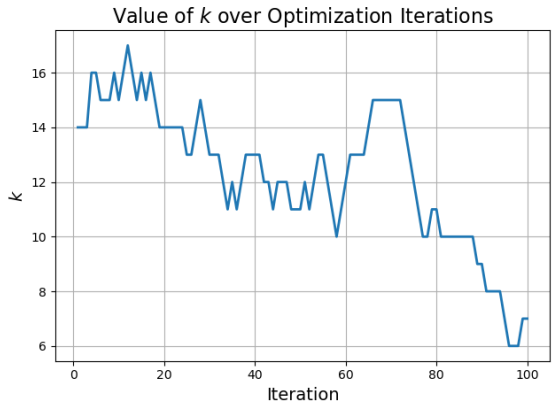

(b) Value of k over 100 iterations of the optimization algorithm

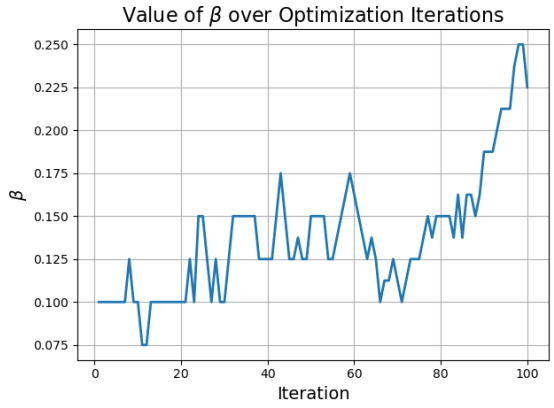

(c) Value of β over 100 iterations of the optimization algorithm

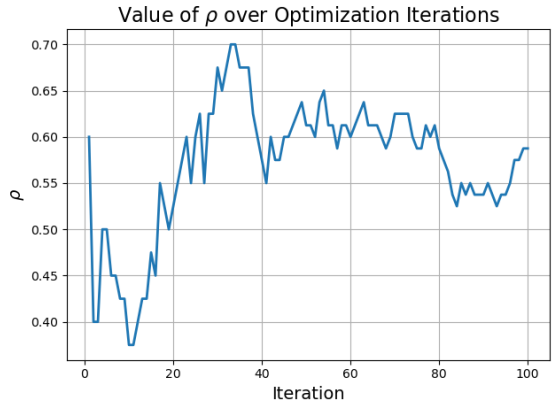

(d) Value of ρ over 100 iterations of the optimization algorithm

Figure 5: Evolution of the optimization process with adaptive reduction of the search space over 100 iterations.

iterations. Indeed, the RMSE looks really noisy probably due to an insufficient amount of averaging

in the estimation of the value at each iteration. In particular, it means that for the same graph and configuration there is an uncertainty of more than one unit.

Moreover, the algorithm explores many different combinations of k, β and ρ during the optimization process. Given that none of these shows a particular advantage over the others in terms of the RMSE, which is the metric we are trying to minimize, we can assume that it is just a coincidence that the values in Table 1 look so similar.

Finally, it is important to notice that the way we compute the RMSE during the optimization process is bound to underestimate the real value. In fact, as we previously argued, there are many sets of parameters with a similar performance and the algorithm relies on very noisy estimates. Assuming that, at each iteration, we have multiple equivalent sets of parameters, we increase the chance that at least one of them is significantly smaller than the real average, and, by the way the algorithm is written, we choose that estimate. This inevitably leads to some selection bias.

Intuitively, if we assume that many configurations are equivalent and the error on the RMSE has a Gaussian shape (i.e. we have unbiased error), the RMSE we are computing, which the minimum over multiple samples, will, on average, lie on the left half of this normal distribution, leading to an underestimation of the mean.

Indeed, the values that we observe during the optimization process look mostly between 3.5 and 5, but when we compute a more reliable estimation, over 30 graphs and 1000 iterations each, we obtain a more accurate estimation of the RMSE of 6.084.

Problem 5

During this problem we aim at improving the performance of Algorithm 2 and we want to evaluate the performance of different types of graphs.

Improvements on the algorithm

First, as we observed in the previous section, the main weakness of the current algorithm is the noisy nature of the RMSE estimation, which confuses the minimization process and hinder the convergence. For this reason, we think that with the current level of noise it would be hard for any method to converge meaningfully past the current point. Let us briefly discuss the sources of noise. First, the architecture of the graph is stochastic, and this introduces some amount of noise. Secondly, the evolution of the epidemic on a given graph depends on the initial position of the infected nodes, and on the spread of the infection, guided by ρ and β. Therefore, an improved version could, at each iteration, average the results on multiple graphs, increase the number of simulations per graph or both. Indeed, our proposed version of the algorithm implements an additional internal cycle, creating multiple graphs, as shown in lines 12-22 of Algorithm 3. When we used it, as discussed below, we also increased the number of simulations per graph.

There are some other notable things in the algorithm, aside from the addition of the stopping criterion based on the maximum number of halvings. First, we use halving as we previously proposed. However, we do not perform it every time we repeat the same best values for twice in a row. Instead, we set an hyperparameter `max_rep` and we halve the step whenever we encounter values seen in the past for at least this number of times. This is done to avoid over reliance on a single value repetition based on possibly inaccurate estimates of the RMSE to decide that convergence at the current step size has been achieved. In practice, we keep a buffer of all the previous best configurations, and whenever we re-encounter some of them we increase a counter. When this counter goes beyond a threshold it gets reset and we halve the step.

Finally, to avoid computing the RMSE for the whole grid we reduce the computational cost to speed up convergence, by sampling only some of the grid elements. In particular, we set the hyperparameter `max_params` and at each iteration we test at most only this number of elements in the grid. To make sure that the logic about the repetitions mentioned above is well posed, we always ensure that the previous best response is included in the current evaluation.

The whole algorithm is shown in Algorithm 3. As a technical note, in order to speed up the computation of lines 12-22, in our actual code implementation we implemented parallelization on the CPU. Notice also that the algorithm is written in a general form, because we will use it also to test different graphs (hence why we substituted k, β, ρ with $\mathbf{x}$.

Hyperparameters used in all the tests

For reproducibility, we report below the values we chose as Algorithm 3 hyperparameters:

$$\texttt{max\_iter} = 100 \quad N_{\text{sim}} = 40, \quad N_{\text{graphs}} = 5,$$
$$\texttt{max\_rep} = 4, \quad \texttt{max\_halvings} = 2, \quad \texttt{max\_params} = 12.$$

Evaluation of the quality of the algorithm

We first wish to evaluate the quality of Algorithm 3 against the results shown in Problem 4. In particular, we can compare the RMSE and the final shape. First, our algorithm reduced significantly the final RMSE to 5.493. We show the full comparison in Table 2.

	Algorithm 2	Algorithm 2 with adaptive halving	Algorithm 3
k^*	8	7	8
β^*	0.2	0.225	0.175
ρ^*	0.6	0.588	0.45
RMSE	6.149	6.084	**5.493**

Table 2: Results of the optimization using Algorithm 2, the adaptive method proposed in Problem 4, and Algorithm 3.

In Figure 6 we can observe that the shape of the graph is slightly more adherent to the ground truth, even though it is far from perfect. We suspect that this might be caused by the underlying model of preferential attachment and it might be impossible to fix. Notably, the extent to which RMSE underestimates the real value is now much smaller, due to the larger number of samples used to estimate it at each iteration and the optimization process looks less noisy.

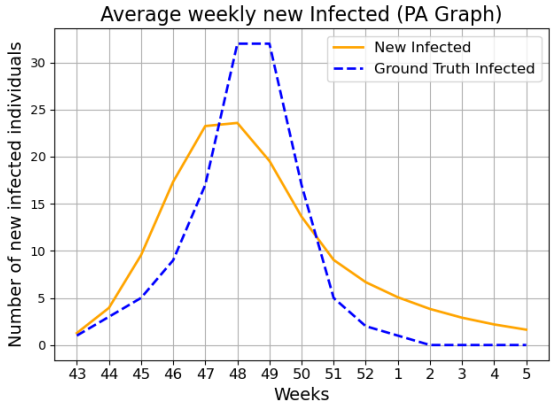

(a) Weekly new estimated infected compared with the ground truth $I_0(t)$, averaged over $N = 1000$ simulations and 30 graphs.

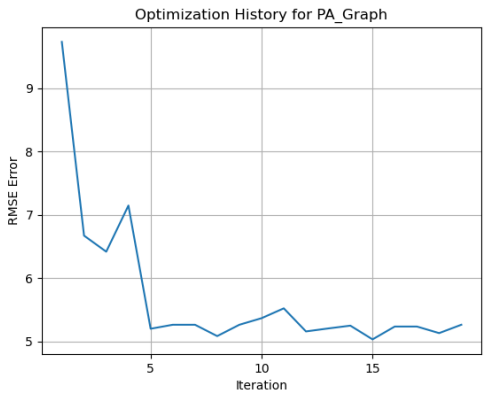

(b) Estimate of the RMSE during the optimization process with Algorithm 3.

Figure 6: Results of the simulation with preferential attachment optimized with Algorithm 3.

Choice of alternative random graphs

We observed before that the main issue with the preferential attachment graph was that it started too early. So, when choosing alternative models, we looked for models that could correct this factor.

Non-linear preferential attachment graph

Given that our previous tests were conducted on a preferential attachment graph, it only seemed natural to test on this one, which relaxes the criterion with which nodes are chosen for the edges. In particular, it depends upon a parameter α and each added node chooses with probability

$$p_j = \frac{d_j^\alpha}{\sum_{v \in \mathcal{V}} d_v^\alpha}$$

where d_i for $i \in \mathcal{V}$ denotes the degree of node i. In particular, if $\alpha > 1$ it increases the degree of the hubs, while if $\alpha < 1$ it decreases it, making the graph more regular. Obviously, given our previous considerations, we would expect $\alpha < 1$.

Configuration model with power-law degrees

This model generates a random graph with a prescribed expected degree sequence following a truncated power law. Let w_i denote the expected degree of node $i \in \mathcal{V}$, sampled from a power-law distribution with exponent γ and truncated to the range $[k_{\min}, k_{\max}]$. Edges are then placed independently between nodes i and j with probability

$$p_{ij} = \frac{w_i w_j}{\sum_{v \in \mathcal{V}} w_v}.$$

This can serve as an alternative to the preferential attachment model. In particular, the presence of maximum value of k could delay the initial steepness.

Erdős-Rényi graph

This is one of the most basic random graphs. It does not create hubs but neither tries to facilitate a k-regular structure as in small world models. This method also serves as a baseline to understand whether these structural assumptions are actually improving the quality of the simulation or not.

Watts-Strogatz model

This is one of the most widely used small world models. It starts with a k-regular graph, which is then modified in such a way that each edge can be rewired with probability p.

Expected results

We expect two different kinds of behavior. In general, we expect that the configuration model and the non-linear PA graph should have a steeper peak, due to the presence of hubs. In fact, once infected, these nodes should significantly speed up the infection process, as also shown in previous points. On the other hand, we expect ER and WS models to have a less steep curve, given the lack of such hubs.

Tests on different graphs

We performed our testing on the graphs described above, using Algorithm 3 to optimize the parameters of the simulation. In particular, we used the non-linear preferential attachment model, the Erdős–Rényi (ER) model, the configuration model (CM) using a power law as the degree distribution and the Watts-Strogatz (WS) model. The results of the convergence values, number of iterations and RMSE are shown in Table 3. Notice that all the methods outperformed our baseline of the preferential

attachment. Unexpectedly, we found that this is also the case for the Erdős–Rényi model, which makes no assumptions over the distribution of the edges, aside for the average degree.

Graph model	**Parameters**	**Iterations**	**RMSE**
Non-linear PA	$(k, \beta, \rho, \alpha) = (8, 0.25, 0.675, 0.4)$	26	5.188
Erdős-Rényi (ER)	$(k, \beta, \rho) = (14, 0.175, 0.95)$	**20**	<u>4.951</u>
Configuration model (CM)	$(k, \gamma, \beta, \rho) = (12, 2.675, 0.15, 0.6)$	32	4.965
Watts-Strogatz (WS)	$(k, p, \beta, \rho) = (18, 0.225, 0.15, 1.0)$	<u>25</u>	**4.896**

Table 3: Performance of different kinds of graphs optimized with Algorithm 3.

In Figure 7 we compare the shape of the estimated weekly new infected with the ground truth. Observe that Watts-Strogatz exhibits a more balanced evolution due to the lack of hubs in the configurations on average, which also looks to be the case for the ER graph. Conversely, the non-linear PA and the configuration model show steeper growth and decay curves. Overall, the results are coherent with the ones we expected, but it is unclear which model yields better results, as they all lack in some regard.

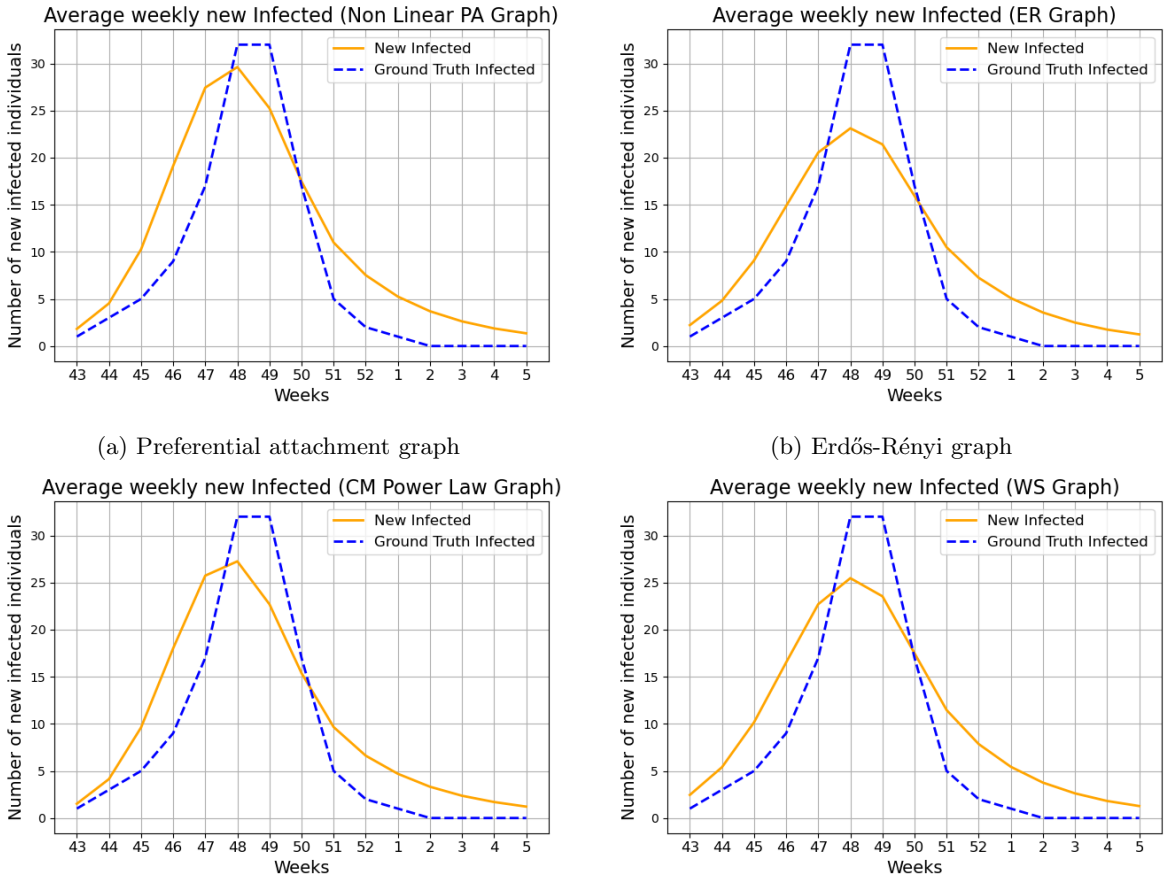

(a) Preferential attachment graph

(b) Erdős-Rényi graph

(c) Configuration model with power law

(d) Watts-Strogatz model

Figure 7: Comparison of the average weekly curve of the estimated new infected nodes compared with teh ground truth. Each plot contains the average evolution over 30 graphs and 1000 simulations each.

Algorithm 3 Grid-based parameter search with multiple graphs and stochastic descent

Require: Initial parameters $\mathbf{x_0}$, step sizes $\Delta\mathbf{x}$, maximum number of iterations `max_iter`
Require: Number of simulations $N_{\text{sim}} = 40$, ground truth data $\{I_0(t)\}_{t=1}^{15}$, number of graphs $N_{\text{graphs}} = 5$, maximum number of parameter combinations to test `max_params`
Require: Maximum number of repetitions `max_rep`, maximum number of halvings `max_halvings`
Ensure: Estimated parameters $\mathbf{x}^*$

converged $\leftarrow$ **false**
$n_{rep} \leftarrow 0$
while not converged **do**
  $\text{RMSE}_{\text{min}} \leftarrow +\infty$
  $\mathbf{x}^* \leftarrow \mathbf{x_0}$
  `it_counter` $\leftarrow 0$
  Compute the full parameter grid: `full_grid` $\leftarrow \prod_{i=1}^{card(\mathbf{x})}\{x_i - \Delta x_i,\ x_i,\ x_i + \Delta x_i\}$
  Sample $\min\{|$`full_grid`$|,$ `max_params`$\}$ elements from `full_grid` and store them in `sampled_grid`
  if $\mathbf{x_0}$ is not in `sampled_grid` **then**
    `sampled_grid` $\leftarrow$ `sampled_grid` $\cup \{\mathbf{x_0}\}$
  end if
  for P in `sampled_grid` **do**
    `it_counter` $\leftarrow$ `it_counter` $+ 1$
    for $j \in \{1, \ldots, N_{\text{graphs}}\}$ **do**
      Generate a graph $G_i = (\mathcal{V}_i, \mathcal{E}_i)$ with the parameters from $P \setminus \{\beta, \rho\}$ used for the graph with $|\mathcal{V}_i| = 934$
      for $i = 1, \ldots, N_{\text{sim}}$ **do**
        Simulate the pandemic on G_i from week 42 for 15 weeks using parameters (β, ρ) from P
        Record weekly new infections $I_{ij}(t)$
      end for
    end for
    Compute average weekly infections: $I(t) \leftarrow \frac{1}{N_{\text{sim}} N_{\text{graphs}}} \sum_{j=1}^{N_{\text{graphs}}} \sum_{i=1}^{N_{\text{sim}}} I_{ij}(t)$
    Compute RMSE: $\text{RMSE} \leftarrow \sqrt{\frac{1}{15}\sum_{t=1}^{15}\big(I(t) - I_0(t)\big)^2}$
    if $\text{RMSE} < \text{RMSE}_{\text{min}}$ **then**
      $\text{RMSE}_{\text{min}} \leftarrow \text{RMSE}$
      $(k^*, \beta^*, \rho^*) \leftarrow (k, \beta, \rho)$
    end if
  end for
  if $\mathbf{x}^*$ has been repeated **then**
    Increase number of repetitions: $n_{rep} \leftarrow n_{rep} + 1$
    if $n_{rep} \geq$ `max_rep` **then**
      Halve the parameters
      $n_{rep} \leftarrow 0$
    end if
  else
    $\mathbf{x_0} \leftarrow \mathbf{x}^*$
  end if
  if performed more halvings than `max_halvings` or `it_counter` $\geq$ `max_iter` **then**
    converged $\leftarrow$ *true*
  end if
end while
return $\mathbf{x}^*$

Exercise 2

Game description and interpretation

We consider a finite game $(V, A, \{u_i\}_{i \in V})$ with player set

$$V = \{1, 2, \dots, n\},$$

where each player chooses an action from the binary action set

$$A = \{-1, +1\}.$$

The set of players is partitioned into two disjoint classes,

$$V_1 = \{1, \dots, n_1\}, \qquad V_2 = \{n_1 + 1, \dots, n\},$$

with $n_1 < n$. The utility functions are defined as follows:

$$u_i(x_i, x_{-i}) = \begin{cases} \dfrac{1}{2} \displaystyle\sum_{j \neq i} |x_i + x_j|, & \text{if } i \in V_1, \\ \dfrac{1}{2} \displaystyle\sum_{j \neq i} |x_i - x_j|, & \text{if } i \in V_2, \end{cases}$$

where $x = (x_1, \dots, x_n) \in A^n$ denotes the action profile.

Players in V_1 are therefore engaged in a *network coordination game*: their payoff is increasing in the number of players choosing the same action. In contrast, players in V_2 face a *network anti-coordination game*, as their utility increases when their action differs from that of the others. These two objectives are inherently opposed: while coordination players benefit from action alignment, anti-coordination players benefit from action differentiation.

In the present setting, each player interacts simultaneously with all other players in the population. From a network perspective, this corresponds to a game played on a *complete graph*, where every node is connected to every other node. For illustration, Figure 8 depicts a complete graph with three nodes.

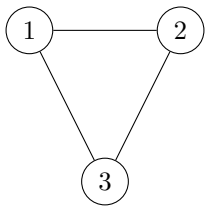

Figure 8: Complete graph with three players.

Given an action profile x_{-i} of the other players, the best response of player i depends on her class. For players in V_1, the utility function rewards agreement with others. Since

$$|x_i + x_j| = \begin{cases} 2, & \text{if } x_i = x_j, \\ 0, & \text{if } x_i \neq x_j, \end{cases}$$

a player in V_1 maximizes her payoff by choosing the action that coincides with the majority of the other players' actions. Formally, letting

$$S_{-i} = \sum_{j \neq i} x_j,$$

the best response correspondence for $i \in V_1$ is

$$\mathrm{BR}_i(x_{-i}) = \begin{cases} \{+1\}, & \text{if } S_{-i} > 0, \\ \{-1\}, & \text{if } S_{-i} < 0, \\ \{-1, +1\}, & \text{if } S_{-i} = 0. \end{cases}$$

Thus, coordination players follow a majority rule, with indifference arising only when the actions of the others are perfectly balanced.

For players in V_2, the logic is exactly reversed. Since

$$|x_i - x_j| = \begin{cases} 2, & \text{if } x_i \neq x_j, \\ 0, & \text{if } x_i = x_j, \end{cases}$$

their payoff is maximized by choosing the action that differs from as many other players as possible. Consequently, a player in V_2 prefers to adopt the action opposite to the majority. The best response correspondence for $i \in V_2$ can therefore be written as

$$\mathrm{BR}_i(x_{-i}) = \begin{cases} \{-1\}, & \text{if } S_{-i} > 0, \\ \{+1\}, & \text{if } S_{-i} < 0, \\ \{-1, +1\}, & \text{if } S_{-i} = 0. \end{cases}$$

Hence, while players in V_1 are driven toward global alignment, players in V_2 are systematically incentivized to deviate from it.

Problem 1: Nash equilibria for $n = 3$ and different class sizes

We now determine the Nash equilibria of the game for $n = 3$ under four different compositions of coordination players, i.e., different values of $n_1 = |V_1|$. Since the action set is binary, $A = \{-1, +1\}$, the equilibrium analysis can be carried out by enumerating the 2^3 action profiles and checking unilateral deviations via the best-response characterizations derived above. Denote the action profile by $x = (x_1, x_2, x_3)$.

(a1) $n_1 = 3$ **(pure coordination).** When $n_1 = 3$, we have $V_1 = V$ and every player has a coordination incentive: player i receives a contribution of 2 from each other player who matches her action and 0 otherwise. Hence any player strictly prefers to match the (strict) majority of the other two players, and is indifferent only under a tie, which cannot occur here because each player faces exactly two opponents. As a consequence, the only profiles with mutual best responses are the two consensus configurations:

$$(-1, -1, -1) \quad \text{and} \quad (+1, +1, +1).$$

These are precisely the Nash equilibria, and they reflect the standard outcome of a majority/coordination game on a complete graph: full alignment is self-reinforcing, while any mixed profile leaves at least one player with a profitable deviation toward agreement.

(a2) $n_1 = 2$ **(two coordinators and one anti-coordinator).** When $n_1 = 2$, two players belong to V_1 and one player belongs to V_2. Without loss of generality, let $V_1 = \{1, 2\}$ and $V_2 = \{3\}$. Players 1 and 2 best respond by matching the majority among the other two players, while player 3 best responds by choosing the opposite of that majority. In equilibrium, players 1 and 2 must align with each other: if $x_1 \neq x_2$, then each coordinator faces a strict majority equal to x_3 and would prefer to match x_3, contradicting equilibrium. Thus $x_1 = x_2$, and then player 3 strictly prefers to pick the opposite action. Therefore, the Nash equilibria are exactly the two profiles in which the two coordinators agree and the anti-coordinator deviates:

$$(-1, -1, +1) \quad \text{and} \quad (+1, +1, -1).$$

Intuitively, the pair in V_1 forms a stable majority of size 2/3 and has no incentive to move, while the single anti-coordination player optimally "breaks" the consensus.

(a3) $n_1 = 1$ **(one coordinator and two anti-coordinators).** When $n_1 = 1$, there is a single coordination player and two anti-coordination players. Let $V_1 = \{1\}$ and $V_2 = \{2, 3\}$ w.l.o.g. The structure of best responses implies that the two anti-coordination players cannot both simultaneously differ from both opponents (because there are only two actions). In any equilibrium, they must therefore take opposite actions, i.e., $x_2 \neq x_3$, so that each of them differs from exactly one opponent and matches the other. Given $x_2 \neq x_3$, player 1 (the coordinator) faces a tie among the others ($S_{-1} = x_2 + x_3 = 0$) and is indifferent between $+1$ and -1, i.e., both are best responses. This indifference doubles the number of equilibria: for each anti-coordination split $(x_2, x_3) = (-1, +1)$ or $(+1, -1)$, the coordinator may choose either action without creating a profitable deviation. Hence the Nash equilibria are:

$$(-1, -1, +1), \quad (-1, +1, -1), \quad (+1, -1, +1), \quad (+1, +1, -1).$$

The increase in equilibrium multiplicity is driven by the appearance of ties in the coordinator's best-response problem, which do not arise when a coordinator faces an even number of opponents.

(a4) $n_1 = 0$ **(pure anti-coordination).** When $n_1 = 0$, we have $V_2 = V$ and the game becomes a pure anti-coordination game on a complete graph with three players. A player's payoff increases with the number of opponents choosing the opposite action; with binary actions and three players, perfect anti-coordination is impossible (at least two players must coincide). In equilibrium, the only stable configurations are those with a 2–1 split: two players choose one action and the remaining player chooses the opposite. Indeed, if all three chose the same action, any player could deviate and increase her payoff by differing from two opponents. In a 2–1 split, the minority player already differs from both others and strictly prefers not to deviate, while each majority player differs from exactly one opponent and is indifferent between staying or switching (switching would simply exchange who is in the minority). Therefore, every profile with exactly one "minority" player is a Nash equilibrium. There are 3 choices of the minority player and 2 choices for the minority action, yielding $3 \times 2 = 6$ equilibria:

$$(-1, -1, +1),\ (-1, +1, -1),\ (+1, -1, -1),\ (+1, +1, -1),\ (+1, -1, +1),\ (-1, +1, +1).$$

In other words, equilibrium corresponds to "as much disagreement as feasible" given the binary action constraint, and the equilibrium set consists of all maximally anti-coordinated (but not perfectly anti-coordinated) configurations.

Problem 2 (b1): Asynchronous BR and noisy BR for $n = 3$, $n_1 = 3$, starting from $X(0) = (+1, -1, +1)$

In case $n = 3$ and $n_1 = 3$ we have $V_1 = V$ (pure coordination on the complete graph). We study the continuous-time dynamics: each player has an independent Poisson clock of rate 1; when player i's clock rings, it updates its action according to the specified rule. The state space is $\{-1, +1\}^3$ and the initial condition is $X(0) = (+1, -1, +1)$.

1. Asynchronous best response (BR) dynamics and transition graph.

In a coordination game on a complete graph with $n = 3$, player i prefers to match as many opponents as possible. If the other two players agree, $x_j = x_k$, then the best response is unique and equals that common value; if the other two disagree, player i is indifferent and both actions are best responses. Under asynchronous BR, when player i is indifferent it selects uniformly among her best responses.

To keep the transition graph readable, we represent only the states that are reachable from the initial condition by best-response updates, and we label each directed edge with its *continuous-time transition rate*.

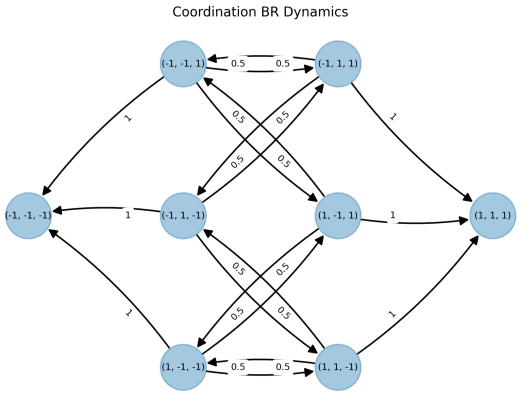

Figure 9: Transition graph for Coordination Game (BR dynamics). The system moves hierarchically towards the two absorbing consensus states (sinks) at the top and bottom.

The transition graph in Figure 9 illustrates the hierarchical flow of the dynamics. The initial state $(+1, -1, +1)$ is situated in the middle layer. From here, the system can flow towards the absorbing consensus states $(+1, +1, +1)$ and $(-1, -1, -1)$. The rates shown on the edges come directly from the clock mechanism: each player is selected at rate 1. For instance, from $(+1, -1, +1)$, player 2 has a *strict* best response to switch to $+1$ (moving to the sink $(+1, +1, +1)$) at rate 1. Meanwhile, players 1 and 3 are indifferent (their two opponents disagree), hence each flips with rate $1 \cdot \frac{1}{2} = \frac{1}{2}$, producing transitions to $(-1, -1, +1)$ and $(+1, -1, -1)$.

Analysis of Hitting Probabilities in Best Response Dynamics The Markov chain associated with the Asynchronous Best Response (BR) dynamics is reducible. Specifically, the states $S_+ = (+1, +1, +1)$ and $S_- = (-1, -1, -1)$ are absorbing states (strict Nash Equilibria), while all other states in the reachable subgraph are transient. Consequently, the limiting distribution as $t \to +\infty$ is concentrated on $\{S_+, S_-\}$. The probability of absorption depends entirely on the initial state $X(0)$.

Let $\tau_y = \inf\{t \geq 0 : X(t) = y\}$ denote the hitting time of state y. We define the hitting probability $h(x)$ as the probability of reaching the positive consensus S_+ before the negative consensus S_- starting from x:

$$h(x) \;=\; \mathbb{P}\big(\tau_{S_+} < \tau_{S_-} \;\mid\; X(0) = x\big).$$

The boundary conditions are $h(S_+) = 1$ and $h(S_-) = 0$. For any transient state x, $h(x)$ satisfies the harmonic property with respect to the transition probabilities P_{xy} of the embedded jump chain:

$$h(x) = \sum_{y \in \mathcal{X}} P_{xy}\, h(y). \tag{1}$$

Since the game is played on a complete graph, the system is symmetric with respect to permutations of players. The state space can be partitioned into equivalence classes based on the number of players choosing action -1, denoted by $k(x) = |\{i : x_i = -1\}|$:

- **Class** S_+ $(k = 0)$: The state $(+1, +1, +1)$. By definition, $h(S_+) = 1$.
- **Class** A $(k = 1)$: States with exactly one -1 (e.g., $x_0 = (+1, -1, +1)$). By symmetry, let $h(x) = p$ for all $x \in A$.

- **Class** B ($k = 2$): States with exactly two -1's (e.g., $y_0 = (-1, -1, +1)$). By symmetry, let $h(x) = q$ for all $x \in B$.
- **Class** S_- ($k = 3$): The state $(-1, -1, -1)$. By definition, $h(S_-) = 0$.

Our objective is to compute $p = h(x_0)$.

We compute the transition rates λ for the Continuous Time Markov Chain (CTMC) and the resulting transition probabilities P for the embedded discrete-time chain. Recall that players activate with rate 1. If a player is indifferent ($|BR_i| = 2$), they switch action with probability 1/2, resulting in an effective transition rate of $1 \cdot 0.5 = 0.5$. If a player has a strict incentive ($|BR_i| = 1$), they switch with rate 1.

Consider the representative state $x_0 = (+1, -1, +1)$.

- **Player 2** (action -1): Observes two opponents playing $+1$. The best response is unique ($BR_2 = \{+1\}$). Player 2 switches to $+1$ with rate $\lambda_2 = 1$. The system moves to S_+.
- **Players 1 and 3** (action $+1$): Observe opponents playing $\{+1, -1\}$. They are indifferent ($BR = \{-1, +1\}$). Each switches to -1 with rate 0.5. The system moves to class B.

The total exit rate from class A is $\Lambda_A = 1 + 0.5 + 0.5 = 2$. The transition probabilities are:

$$P(A \to S_+) = \frac{1}{2}, \qquad P(A \to B) = \frac{0.5 + 0.5}{2} = \frac{1}{2}.$$

Applying the harmonic equation (1) to p:

$$p = \frac{1}{2}h(S_+) + \frac{1}{2}h(B) \quad \Longrightarrow \quad p = \frac{1}{2}(1) + \frac{1}{2}q \quad \Longrightarrow \quad 2p = 1 + q. \tag{2}$$

Consider the representative state $y_0 = (-1, -1, +1)$.

- **Player 3** (action $+1$): Observes two opponents playing -1. The best response is unique ($BR_3 = \{-1\}$). Player 3 switches to -1 with rate $\lambda_3 = 1$. The system moves to S_-.
- **Players 1 and 2** (action -1): Observe opponents playing $\{-1, +1\}$. They are indifferent. Each switches to $+1$ with rate 0.5. The system moves to class A.

The total exit rate is $\Lambda_B = 2$. The transition probabilities are:

$$P(B \to S_-) = \frac{1}{2}, \qquad P(B \to A) = \frac{1}{2}.$$

Applying the harmonic equation to q:

$$q = \frac{1}{2}h(S_-) + \frac{1}{2}h(A) \quad \Longrightarrow \quad q = \frac{1}{2}(0) + \frac{1}{2}p \quad \Longrightarrow \quad q = \frac{1}{2}p. \tag{3}$$

We solve the linear system formed by equations (2) and (3):

$$\begin{cases} 2p = 1 + q \\ q = \frac{1}{2}p \end{cases} \quad \Longrightarrow \quad 2p = 1 + \frac{1}{2}p \quad \Longrightarrow \quad \frac{3}{2}p = 1 \quad \Longrightarrow \quad p = \frac{2}{3}.$$

Substituting back, we find $q = 1/3$.

Starting from the configuration $X(0) = (+1, -1, +1)$, the probability that the Best Response dynamics converges to the positive consensus equilibrium is:

$$\lim_{t \to +\infty} \mathbb{P}\big(X(t) = S_+ \mid X(0) = (+1, -1, +1)\big) = \frac{2}{3}.$$

Conversely, the probability of converging to the negative consensus is 1/3. Since the process is absorbed into $\{S_+, S_-\}$ with probability 1, the limiting probability of any other configuration $x \notin \{S_+, S_-\}$ is zero:

$$\forall x \notin \{S_+, S_-\}, \quad \lim_{t \to +\infty} \mathbb{P}\big(X(t) = x\big) = 0.$$

Experimental Validation. To confirm the theoretical derivation, we performed a frequency analysis over $N = 5000$ independent simulation runs. Each run consisted of 50 steps starting from the initial configuration $x_0 = (+1, -1, +1)$. The empirical results (Figure 10) are highly consistent with the analytical predictions:

- Frequency of convergence to $(-1, -1, -1)$: 0.3408 (Theoretical: $1/3 \approx 0.3333$).
- Frequency of convergence to $(+1, +1, +1)$: 0.6592 (Theoretical: $2/3 \approx 0.6667$).
- Frequency of remaining in transient configurations: ≈ 0.

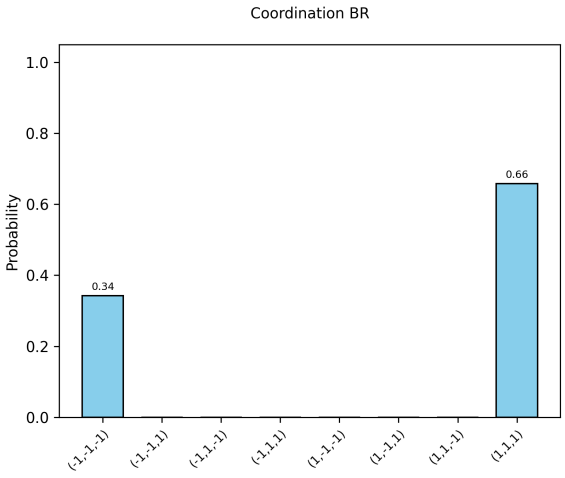

Figure 10: **Coordination BR**: Empirical frequency of absorption (5000 runs) starting from $(+1, -1, +1)$. The system is absorbed into the $(+1, +1, +1)$ consensus approximately 2/3 of the time, and into $(-1, -1, -1)$ approximately 1/3 of the time.

2. Noisy best response (NBR) dynamics and vanishing-noise limit.

In the noisy best response dynamics, when player i's clock rings it chooses $a \in \{-1, +1\}$ with logit probabilities

$$\mathbb{P}\big(x_i(t^+) = a \,\big|\, X(t) = x\big) = \frac{e^{\eta\, u_i(a, x_{-i})}}{e^{\eta\, u_i(+1, x_{-i})} + e^{\eta\, u_i(-1, x_{-i})}},$$

where $\eta > 0$ is the inverse-noise parameter (larger η means decisions are more concentrated on best responses).

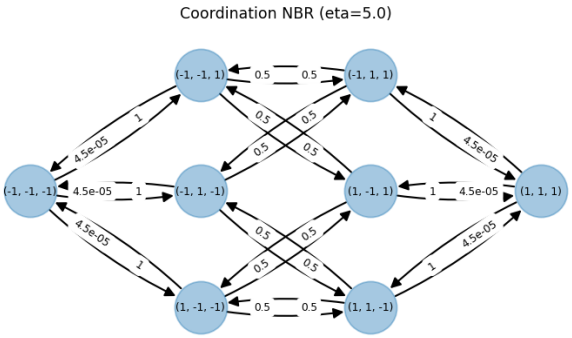

Figure 11: Transition graph for Coordination Game (NBR dynamics, $\eta = 5.0$).

The transition graph for NBR is shown in Figure 11. We observe that while the structure is similar to the BR case, the noise allows for "uphill" transitions, making the system ergodic and enabling it to escape local traps over long time horizons.

For every fixed η, this chain is irreducible and aperiodic on the finite state space $\{-1,+1\}^3$, hence it admits a unique invariant distribution π_η, and

$$\lim_{t\to+\infty} \mathbb{P}\big(X(t)=x \,\big|\, X(0)=x^0\big) = \pi_\eta(x) \qquad \text{for all initial states } x^0.$$

In the coordination case ($n_1 = 3$), the game is a potential game. A convenient potential is the number of agreeing pairs

$$\Phi(x) = \sum_{1\le i<j\le 3} \mathbf{1}\{x_i = x_j\},$$

which attains its global maximum exactly at the two consensus states $(+1,+1,+1)$ and $(-1,-1,-1)$. The logit dynamics induces a Gibbs-type invariant measure of the form

$$\pi_\eta(x) = \frac{e^{\eta\,\Phi(x)}}{\sum_{y\in\{-1,+1\}^3} e^{\eta\,\Phi(y)}},$$

In the vanishing noise limit ($\eta\to\infty$), the probability mass of the invariant distribution concentrates exclusively on the set of states that maximize the potential function. Since the potential $\Phi(x)$ depends only on the number of agreeing pairs, the game is symmetric with respect to the label of the actions. The global maximum of the potential is attained uniquely at the two consensus configurations:

$$\Phi(+1,+1,+1) \;=\; \Phi(-1,-1,-1) \;=\; \Phi_{\max},$$

while for any other configuration x, we have $\Phi(x) < \Phi_{\max}$. Consequently, as $\eta\to\infty$, the ratio of the probability of a sub-optimal state to a consensus state vanishes exponentially:

$$\frac{\pi_\eta(x)}{\pi_\eta(\pm\mathbf{1})} = e^{-\eta(\Phi_{\max}-\Phi(x))} \xrightarrow{\eta\to\infty} 0, \quad \forall x \notin \{+\mathbf{1},-\mathbf{1}\}.$$

This implies that the limiting distribution is supported entirely on the two consensus states. Furthermore, due to the symmetry of the potential, these two states must have equal probability. Therefore, regardless of the initial configuration $X(0)$, we have:

$$\lim_{\eta\to\infty} \pi_\eta(+\mathbf{1}) = \frac{1}{2}, \qquad \lim_{\eta\to\infty} \pi_\eta(-\mathbf{1}) = \frac{1}{2}.$$

Experimental Validation. We validated the theoretical predictions by performing a continuous-time simulation of the NBR dynamics for $N = 50,000$ steps with a noise parameter $\eta = 5.0$, starting from the configuration $x_0 = (+1,-1,+1)$. The results (Figure 12) confirm that the probability mass is almost entirely concentrated on the two potential maximizers:

$$\hat\pi(-1,-1,-1) \approx 0.49, \qquad \hat\pi(+1,+1,+1) \approx 0.51.$$

The cumulative probability of all other transient configurations is negligible (< 0.001), consistent with the vanishing noise limit prediction.

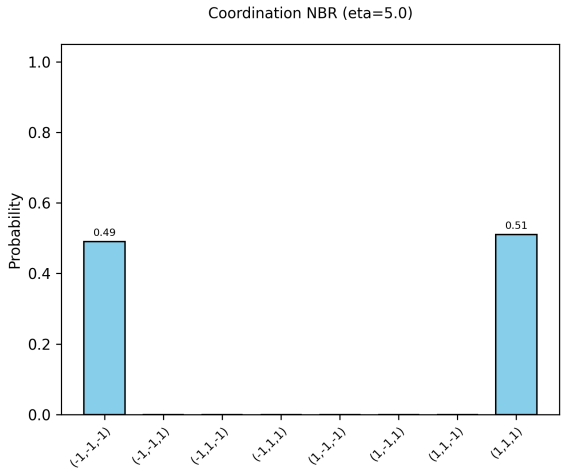

Figure 12: **Coordination NBR**: Long-run time-average distribution ($\eta = 5.0$). Due to noise, the system is ergodic and spends roughly equal time visiting both consensus states.

Problem 2 (b2): Asynchronous BR and noisy BR for $n = 3$, $n_1 = 0$, starting from $X(0) = (+1, -1, +1)$

In case $n = 3$ and $n_1 = 0$, we have $V_2 = V$ (pure anti-coordination on the complete graph). The dynamics are defined similarly, but the utility function now rewards mismatches: $u_i(x) = \sum_{j \neq i} |x_i - x_j|$. The state space is $\{-1, +1\}^3$ and the initial condition is $X(0) = (+1, -1, +1)$.

1. Asynchronous best response (BR) dynamics and transition graph.

In an anti-coordination game on a complete graph with $n = 3$, player i prefers to choose the action opposite to the majority of opponents. If the two opponents disagree ($x_j \neq x_k$), player i faces one opponent playing $+1$ and one playing -1. In this case, choosing $+1$ yields 1 mismatch, and choosing -1 yields 1 mismatch. Thus, player i is always indifferent when opponents disagree. Conversely, if opponents agree ($x_j = x_k$), player i has a strict incentive to choose the opposite action.

We analyze the reachable set from the initial condition $x_0 = (+1, -1, +1)$.

- **Player 2** (action -1): Sees opponents playing $+1, +1$. This is the ideal state (2 mismatches). The best response is unique and is to keep -1.
- **Players 1 and 3** (action $+1$): See opponents playing $+1, -1$. They are indifferent. Under asynchronous BR, they switch action with probability $1/2$ upon activation.

Since no player has a strict incentive to move towards consensus (states $(+1, +1, +1)$ or $(-1, -1, -1)$), these states are unreachable. Instead, the dynamics are confined to the set of "mixed" states (configurations with exactly one mismatching pair).

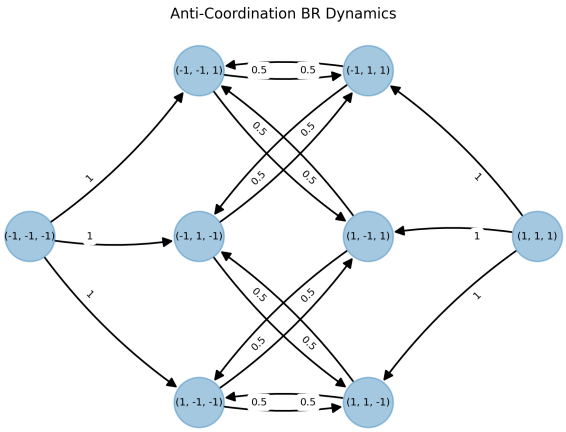

Figure 13: Transition graph for Anti-Coordination Game (BR dynamics). The system is trapped in the set of mixed states and never reaches the consensus states.

The transition graph in Figure 13 visualizes this behavior. The reachable subgraph forms a *closed communicating class* $\mathcal{M}$ consisting of the 6 mixed states. Due to the symmetry of the transition rates and the graph topology (a node-transitive cycle), the invariant distribution is uniform over the reachable states.

$$\lim_{t\to\infty} \mathbb{P}(X(t) = x \mid X(0) = x_0) = \begin{cases} 1/6 & \text{if } x \in \mathcal{M}, \\ 0 & \text{otherwise.} \end{cases}$$

Experimental Validation. Simulation over a single run of $N = 50,000$ steps of confirms this behavior. The system never reached $(-1,-1,-1)$ or $(+1,+1,+1)$. The final states (14) were distributed approximately uniformly among the 6 mixed configurations (frequencies ranging between 0.162 and 0.171), consistent with the theoretical probability of $1/6 \approx 0.1667$.

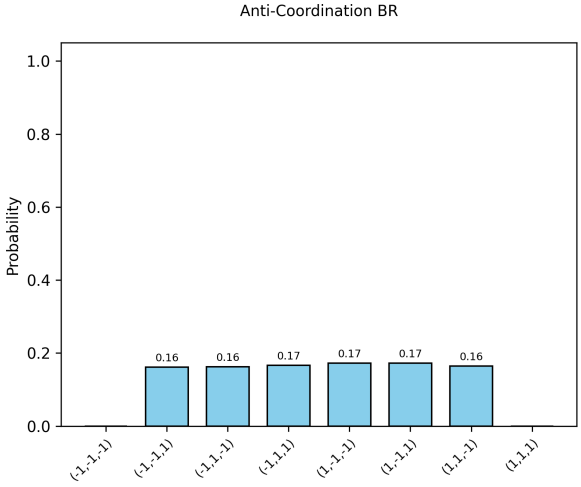

Figure 14: **Anti-Coordination BR**: The system is trapped in a cycle and visits the 6 "mixed" states uniformly. The consensus states $(-1,-1,-1)$ and $(+1,+1,+1)$ are never reached.

2. Noisy best response (NBR) dynamics and vanishing-noise limit.

The NBR dynamics follows the same logit rule as defined in the previous section. In the anti-coordination case, the potential function $\Phi(x)$ counts the number of disagreeing pairs:

$$\Phi(x) = \sum_{1 \le i < j \le 3} \mathbf{1}\{x_i \neq x_j\}.$$

This potential attains its global minimum (0) at the consensus states and its *global maximum* (2) at the 6 mixed states (where exactly one pair agrees and two pairs disagree).

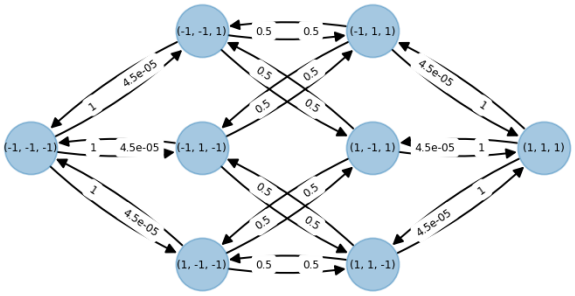

Figure 15: Transition graph for Anti-Coordination Game (NBR dynamics, $\eta = 5.0$). Dominant paths highlight the same cyclic structure as the BR dynamics.

The NBR graph (Figure 15) confirms that the dynamics are statistically concentrated on the potential maximizers. Specifically, for any mixed state $x \in \mathcal{M}$, $\Phi(x) = 2$, while $\Phi(+1,+1,+1) = \Phi(-1,-1,-1) = 0$.

In the vanishing noise limit ($\eta \to \infty$), the invariant distribution concentrates on the set of potential maximizers. Since $\operatorname{argmax}_x \Phi(x) = \mathcal{M}$, and all states in $\mathcal{M}$ have the same potential value, the limiting distribution is uniform over $\mathcal{M}$:

$$\lim_{\eta \to \infty} \pi_\eta(x) = \begin{cases} 1/6 & \text{if } x \in \mathcal{M}, \\ 0 & \text{if } x \in \{(-1,-1,-1), (+1,+1,+1)\}. \end{cases}$$

Experimental Validation. We validated the theoretical predictions by performing a continuous-time simulation of the NBR dynamics for $N = 50,000$ steps with a noise parameter $\eta = 5.0$, starting from the configuration $x_0 = (+1,-1,+1)$. The results (Figure 16) confirm the theoretical expectations:

- The probability mass on the two consensus states was negligible.
- The remaining probability was distributed approximately uniformly among the 6 mixed states, with individual frequencies ranging between 0.165 and 0.168 (theoretical value $1/6 \approx 0.1667$).

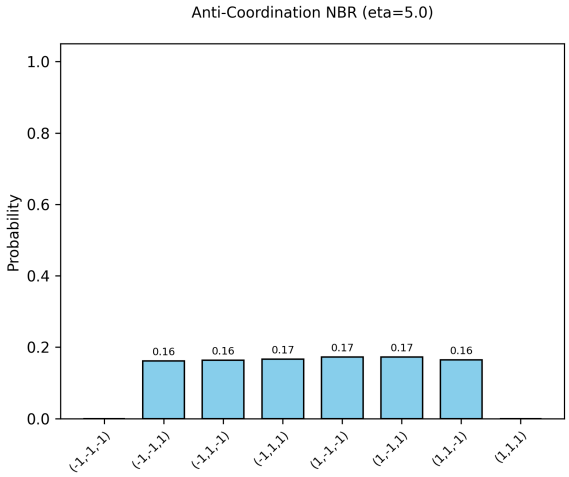

Figure 16: **Anti-Coordination NBR**: Long-run time-average distribution ($\eta = 5.0$). The probability mass concentrates uniformly on the potential maximizers, which are the 6 mixed states.